Natural Occurrence of $MgSiO_3$-Ilmenite and Evidence for $MgSiO_3$-Perovskite in a Shocked L Chondrite

Thomas G. Sharp,* Cornelia M. Lingemann, Catherine Dupas, Dieter Stöffler

Shock-induced melt veins in the Acfer 040 L5-6 (S6) chondrite contain a previously unknown set of high pressure phases consisting of amorphous grains similar in composition to majorite, $MgSiO_3$-ilmenite, and ringwoodite. The amorphous grains have compositions that are similar to those of synthetic $MgSiO_3$-perovskites from chemically complex systems and are inferred to be $MgSiO_3$-perovskite that crystallized from the melt at high pressure and temperature and subsequently amorphized after pressure release. The ilmenite represents a natural occurrence of a potentially important mineral in Earth's mantle. The $MgSiO_3$-perovskite–$MgSiO_3$-ilmenite–ringwoodite assemblage is not predicted by phase equilibria studies, but appears to result from crystallization of a melt at pressures above 26 gigapascals.

The minerals that make up Earth's transition zone (410- to 660-km depth) and lower mantle are inferred primarily from high-pressure experiments (*1*) with only a few natural samples from the deep Earth found as inclusions in diamonds (*2*). The most common natural occurrences of high-pressure mafic minerals are in melt veins within shocked chondrites that formed as a result of shock metamorphism during impact events on chondritic parent bodies. Ringwoodite, the spinel-structure high-pressure polymorph of olivine, was observed in the Tenham L6 chondrite (*3*). Majorite, a high-pressure garnet with a composition near that of enstatite, was observed in the Coorara chondrite (*4, 5*). In his review of pyroxene-garnet reactions, Ringwood (*1*) interpreted the majorite of Coorara (*5*) as a product of crystallization at high pressure during the adiabatic pressure-temperature release after the shock pulse. The modified-spinel polymorph of olivine "wadsleyite" was later found in Tenham (*6*). Melt veins in highly shocked chondrites contain high-pressure minerals that are believed to have crystallized at high pressure during shock events (*1, 7–11*). The high-pressure liquidus assemblage of magnesiowüstite plus majorite, identified in the matrix of melt veins in the Sixiangkou L6 chondrite (*10*), indicates that the mineralogy of melt veins may be useful in interpreting crystallization conditions during shock metamorphism (*10*).

T. G. Sharp, Department of Geology, Arizona State University, Tempe, AZ 85287–1404 USA.
C. M. Lingemann, Institut für Planetologie, Wilhelm-Klemm Str. 10, D-48149 Münster, Germany.
C. Dupas, Bayerisches Geoinstitut, Universität Bayreuth, D-95440 Bayreuth, Germany.
D. Stöffler, Museum für Naturkunde, Invaliden Str. 43, D-10115 Berlin, Germany.
*To whom correspondence should be addressed. E-mail: tom.sharp@asu.edu

Natural occurrences of high-pressure minerals in shocked chondrites are relevant to the mineralogy of Earth's mantle because they provide natural examples of important compounds in Earth. Without such natural examples, synthetic phases considered to be important in Earth's mantle are not considered to be minerals. $MgSiO_3$-perovskite was synthesized by Liu (*12*) and has a distorted perovskite structure. Although $MgSiO_3$-perovskite is inferred to be the most abundant phase in Earth, it has not been found in nature and thus has no mineral name. $MgSiO_3$-ilmenite, which was synthesized by Kawai *et al.* (*13*) and identified as having an ilmenite structure by Liu (*14*), is also a potentially important mantle mineral that has not been previously found in nature.

The high-pressure minerals in shocked chondrites provide an important source of information concerning the pressure, temperature, and duration of shock metamorphism when combined with information from dynamic shock experiments and static high-pressure experiments (*7–11, 15, 16*). The melt veins in shocked chondrites commonly consist of two distinct textural units: (i) "inclusions" of polycrystalline ringwoodite and majorite aggregates with olivine and enstatite compositions similar to those of the host chondrite, and (ii) "matrix" composed of small majorite crystals that are compositionally complex and coexist with minerals such as magnesiowüstite, ringwoodite, wadsleyite, kamacite, and troilite (*10, 11, 15, 16*). The matrix assemblage represents crystallization from the shock-induced melt at high pressure, whereas the polymorphic aggregates represent predominantly solid-state transformations from olivine and pyroxene (*1, 7–11, 15, 16*).

The sample examined in this study is an L5-6 (S6) chondrite known as Acfer 040, which was found in the Algerian Sahara in 1989 (*17*). Our sample is a breccia that contains many black melt veins and melt pockets (*8, 11*). Using the classification of shock metamorphism in ordinary chondrites based on shock-recovery experiments (*18*), this shocked sample may have experienced peak pressures in excess of 60 GPa near the zones of melting. However, such pressure estimates should be made with caution, because the over-pressure required for phase transformations is dependent on the duration of the shock event (*16, 10*). We examined this sample using optical microscopy, electron microprobe analysis, scanning electron microscopy (SEM), and analytical transmission electron microscopy (TEM) (*19*). The Acfer 040 sample was chosen because of its high degree of shock metamorphism (S6) and its high concentration of narrow melt veins. The goal of this study was to characterize the high-pressure mineral assemblages of the melt veins to better understand crystallization conditions.

The matrix of the melt veins consists of a mixture of equant grains of amorphous material, of about 2 μm (1.9 ± 0.4 μm) in size, surrounded by finer mineral grains and interstitial glass (Fig. 1). The amorphous grains are morphologically distinct from the interstitial glass in that they do not fill irregular voids between crystals. Electron diffraction patterns collected from the glassy grains confirm that they are amorphous (Fig. 1), although in some cases these amorphous grains have tiny crystalline inclusions (40 to 250 nm) of FeNi, troilite, or Fe-oxide. EDS analyses of the amorphous grains show that they have a composition similar to that of majorites that commonly occur in the matrix of the melt veins (*5, 9–11*). This composition can be approximated by a solid solution between an end-

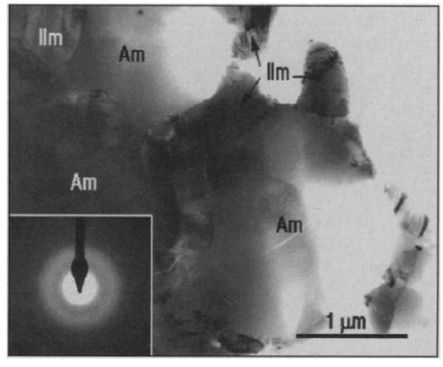

Fig. 1. Bright-field TEM image of the melt-vein matrix showing amorphous grains (Am) surrounded by crystals of $MgSiO_3$-ilmenite (Ilm). The selected-area electron diffraction pattern (**inset**), recorded from the amorphous grain on the right side of the image, has a diffuse ring pattern indicative of electron scattering from an amorphous material.

member majorite ($Mg_3(Mg,Si)_2Si_3O_{12}$) and pyrope ($Mg_3Al_2Si_3O_{12}$) (*10*) with additional FeO, CaO, Na_2O, MnO, and Cr_2O_3. The interstitial glass contains TiO_2 and up to several weight percent P_2O_5, and has more CaO and less FeO than the amorphous grains (Table 1).

The principal crystalline phase between the amorphous grains consists of prismatic or plate-like crystals (Fig. 2) of $MgSiO_3$ with small amounts of FeO, Al_2O_3, Na_2O, and Cr_2O_3 (Table 1). Electron diffraction patterns from this material are consistent with the structure of $MgSiO_3$-ilmenite, a high-pressure polymorph of enstatite (Fig. 3). These patterns could not be indexed with the structure of the other enstatite polymorphs (orthoenstatite, clinoenstatite, high-pressure clinoenstatite, majorite), although some patterns could be indexed as $MgSiO_3$-perovskite. To be certain that the electron diffraction data can only represent the ilmenite structure (space group $R\bar{3}$) and not $MgSiO_3$-perovskite, we collected multiple diffraction patterns from single grains and indexed them all as ilmenite using d-spacings, angles, symmetry, and systematic absences for dynamical diffraction. In addition, we constructed a stereographic projection from a series of electron diffraction patterns to demonstrate that all indexed patterns of a single grain fit the ilmenite structure in three dimensions (Fig. 4). Through this analysis we can also rule out the similar hematite structure (space group $R\bar{3}c$) (*20*). Based on the presence of $\bar{h}h0l$ reflections with $l = 2n + 1$ in the $[11\bar{2}0]$ zone axis diffraction pattern (Fig. 3), we can demonstrate that the diffraction symmetry is consistent with the $R\bar{3}$ space group of ilmenite, but not the $R\bar{3}c$ space group of hematite.

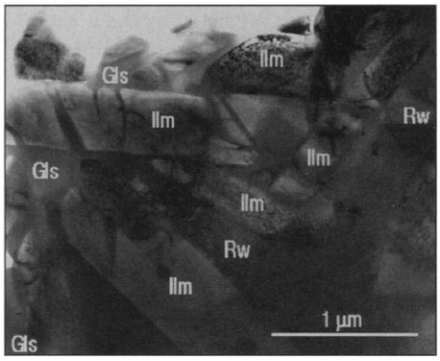

Fig. 2. Bright-field TEM image of numerous $MgSiO_3$-ilmenite (Ilm) and ringwoodite (Rw) grains in a matrix of interstitial glass (Gls). Many of the $MgSiO_3$-ilmenite grains have mottled contrast as well as fracture-like features filled with amorphous material.

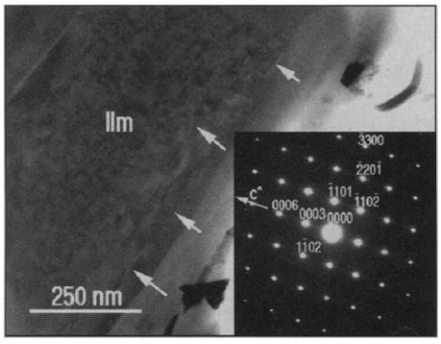

Fig. 3. Bright-field TEM image of an $MgSiO_3$-ilmenite grain (Ilm) obtained with $g = 00012$, showing tiny planar defects (arrows) on the (0001) planes. The SAED pattern (**inset**) of the $[11\bar{2}0]$ zone axis shows streaking along c^*, indicating one-dimensional disorder resulting from the (0001)-planar defects. The SAED pattern also distinguishes the ilmenite structure (space group $R\bar{3}$) from the similar hematite structure ($R\bar{3}c$) by the presence of $\bar{h}h0l$ reflections where $l = 2n + 1$, which are forbidden in the $R\bar{3}c$ space group.

The $MgSiO_3$-ilmenite grains have variable morphologies, with most forming prismatic crystals up to several micrometers long. Many contain tiny planar defects that are visible as small spots or platelets with local strain contrast (Figs. 2 and 3) and that result in faint streaking along c^* in electron diffraction patterns (Fig. 3). The distribution of these defects is heterogeneous, with most occurring within the cores of the ilmenite grains. Diffraction contrast imaging of these defects shows that they are tiny plates on the (0001) planes that are about 80 nm wide and 1 nm thick (Fig. 3). These features are similar in appearance to the Guinier-Preston zones seen in pyroxenes (*21*) and suggest the beginning of homogeneous exsolution. The platelets might consist of corundum or hematite (both minerals have space group $R\bar{3}c$) representing exsolution of excess Al_2O_3 or Fe_2O_3 from $MgSiO_3$. Many of the ilmenite grains also have fracture-like features that are filled with amorphous material (Fig. 2), suggesting that the $MgSiO_3$-ilmenite experienced partial amorphization upon decompression.

The second crystalline phase in the melt-vein matrix is ringwoodite (Figs. 2 and 5). The ringwoodite grains can be either equant or somewhat elongated, ranging in size from about 400 nm to about 1 μm. They show a high degree of stacking disorder indicated by high densities of stacking faults on {110} planes that commonly occur as short (100 to 200 nm) segments. These faults probably represent growth defects that formed during crystallization of disordered ringwoodite. The textural relations between ringwoodite and the ilmenite phase suggest that these two minerals crystallized simultaneously. This is illustrated in (Fig. 5) by a ringwoodite grain that is partially embayed by an ilmenite.

The morphological and compositional differences between the amorphous grains and the interstitial glass are inconsistent with both being quenched remnants of residual melt after partial crystallization. During crystallization of a silicate melt by a homogeneous nucleation mechanism, the distribution of crystal nuclei should be random. The nonrandom distribution of crystals around amorphous grains suggests that

Table 1. Average compositions of amorphous grains (Am. grains), interstitial glass (Int. glass) and $MgSiO_3$-ilmenite based on semiquantitative EDS analyses obtained by analytical electron microscopy. Standard deviations are given in parentheses. Trace amounts (tr) of Cr were noted as tiny $K\alpha$ peaks in the EDS spectra.

Oxide	Am. grains		Int. glass		$MgSiO_3$-ilmenite	
SiO_2	49.14	(0.36)	44.96	(2.33)	55.54	(0.27)
TiO_2			0.50	(0.02)		
Al_2O_3	4.69	(0.42)	3.92	(0.87)	4.44	(0.47)
Cr_2O_3	tr				0.50	(0.19)
FeO	13.16	(0.85)	11.45	(1.28)	3.72	(0.47)
MgO	26.24	(1.07)	26.69	(1.21)	35.34	(0.48)
MnO	0.81	(0.17)	0.92	(0.13)		
CaO	3.95	(0.59)	7.00	(0.83)		
Na_2O	2.02	(0.26)	1.88	(0.29)	0.42	(0.22)
P_2O_5			2.68	(1.42)		
Formula						
O	12				12	
Si	3.61	(0.03)			3.79	(0.02)
Ti						
Al	0.36	(0.12)			0.36	(0.04)
Cr					0.03	(0.01)
Fe	0.81	(0.05)			0.21	(0.03)
Mg	2.87	(0.11)			3.60	(0.05)
Mn	0.05	(0.01)				
Ca	0.31	(0.05)				
Na	0.29	(0.04)			0.06	(0.03)

the amorphous grains were crystalline at the time when the $MgSiO_3$-ilmenite and ringwoodite crystallized. This implies that these relatively large grains, compared to the ilmenite and ringwoodite grains, became amorphous during or after pressure release. Majorite, which is compositionally similar to the amorphous grains, is an unlikely candidate for a precursor crystal because it is a relatively robust mineral that does not become amorphous during thermal quench in static high-pressure experiments or during normal TEM sample preparation (*22*). Natural as well as synthetic majorites are not easily amorphized by electron irradiation during TEM characterization (*8*, *11*, *16*, *22*). Similarly, the precursor phase is unlikely to have been a pyroxene, because the low-pressure pyroxenes are also robust and the high-pressure clinoenstatite transforms readily to low-pressure clinoenstatite (*23*). $MgSiO_3$-perovskite, which can have a composition similar to that of majorite (*24*), is a likely precursor to the amorphous grains because it is unstable at low pressure and readily becomes amorphous. It is known to vitrify at one atmosphere if heated to a temperature greater than 150°C or when prepared for TEM using conventional ion milling settings (*25*). $MgSiO_3$-perovskite is also known to amorphize when crushed at room temperature with a mortar and pestle (*26*). A similar interpretation was made of $MgSiO_3$-rich glass coexisting with magnesiowüstite in a melt vein (*27*). The instability of $MgSiO_3$-perovskite at low pressures combined with the waste heat that remains after shock metamorphism [the post-shock temperature increase for S6 is estimated to be greater than 850°C (*18*)] makes it unlikely that crystalline $MgSiO_3$-perovskite will ever be found in shocked chondrites.

If the amorphous grains represent vitrified $MgSiO_3$-perovskite, their chemical compositions should be similar to those of synthetic $MgSiO_3$-perovskites from chemically complex systems. The amorphous grains are different from $MgSiO_3$-perovskites synthesized at 26 GPa and 1975°C from a carbonaceous chondrite starting material (*28*) because they have higher concentrations of Al_2O_3 than the synthetic material. However, the Al_2O_3 content of the amorphous grains is similar to that of perovskites synthesized from a pyrolite composition at 28 GPa and 1500°C (*24*), and they are within the range of Al_2O_3 contents of $MgSiO_3$ perovskites synthesized at 25 to 26 GPa in the $MgSiO_3$-$Mg_3Al_2Si_3O_{12}$ system (*29*). Another difference between the amorphous grains and the synthetic $MgSiO_3$ perovskites is the high concentration of CaO and Na_2O in the former. The high CaO content may represent a relatively large amount of $CaSiO_3$-perovskite dissolved in the $MgSiO_3$-perovskite because $CaSiO_3$-perovskite is not present. In synthetic samples containing CaO, both perovskite phases are generally present, and therefore most of the CaO is taken up by the $CaSiO_3$-perovskite (*24*, *28*, *29*). Although the Na_2O content is high relative to $MgSiO_3$-perovskites that coexist with magnesiowüstite (*24*, *28*, *29*), the 2% by weight of Na_2O seen in the amorphous grains is the same as that measured in Mg-Al perovskites synthesized from mid-ocean-ridge basaltic glass at 80 and 100 GPa (*30*). Based on the similarity in chemical composition between our amorphous grains and synthetic $MgSiO_3$-perovskite and the highly unstable nature of the $MgSiO_3$-perovskite structure at low pressure, we infer that the amorphous grains in the melt veins of Acfer 040 were chemically complex $MgSiO_3$-perovskite that crystallized from the melt at high pressure and subsequently became amorphous.

The crystallization of the melt vein involved three silicate phases as well as Fe-Ni metal and troilite. The distribution of minerals and glassy grains (Fig. 1) as well as intergrown $MgSiO_3$-ilmenites and ringwoodites (Fig. 5) suggest a sequence of crystallization that started with nucleation and growth of a chemically complex $MgSiO_3$-perovskite followed by the simultaneous nucleation and growth of $MgSiO_3$-ilmenite and ringwoodite. The metal-sulfide melt crystallized later when the temperature had dropped below about 875°C (*28*). The presence of substantial amounts of interstitial glass indicates that the system was rapidly quenched from high pressure and temperature conditions while crystallization was occurring.

The silicate assemblage, consisting of $MgSiO_3$-perovskite, $MgSiO_3$-ilmenite, and ringwoodite is not predicted by the liquidus phase diagram for Allende (*28*), for peridotite (*31*), or for other simpler systems (*32*). In phase equilibrium studies of the $MgSiO_3$ system (*32*), pyroxene, garnet, or perovskite are liquidus phases, whereas $MgSiO_3$-ilmenite is a subsolidus phase. This suggests that the $MgSiO_3$-ilmenite crystallized metastably, probably while the pressure and temperature were rapidly changing in the release phase of shock metamorphism.

The melt vein we investigated is relatively poor in the olivine component and contains considerable P_2O_5. This implies that the melt vein did not have a bulk-chondritic composition as seen by Chen *et al.* (*10*). The minerals that melted to form this vein may have included a large amount of enstatite and plagioclase as well as some apatite. This suggests that chemical heterogeneities may be common in melt veins and that the mixing of molten mineral components is not necessarily complete during melt vein formation. The presence of P_2O_5 may explain the lack of magnesiowüstite that one would expect to coexist with $MgSiO_3$-perovskite. It has been shown that P_2O_5 can have a profound effect on the activity of components and the phases that crystallize in basaltic melts at one atmosphere (*33*) where P_2O_5 increases the activity of SiO_2 and suppresses the crystallization of Fe-oxides. The presence of P_2O_5 in the Acfer 040 melt veins combined with a relatively olivine-poor composition may have suppressed the crystallization of magnesiowüstite. The presence of silicate perovskite in Acfer 040 suggests that crystallization began at a pressure considerably higher than in samples such as Tenham (*9*, *34*, *35*) and Sixiangkou (*10*, *16*), where majorite is the predominant matrix phase in the melt veins. Based on the stability of $MgSiO_3$-perovskite in Allende (*28*), crystallization

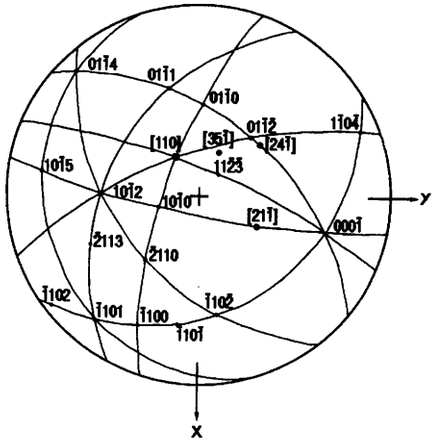

Fig. 4. Stereographic projection of $MgSiO_3$-ilmenite built from four SAED patterns showing that all four patterns match the ilmenite structure in three dimensions. Planes in the ilmenite structure are represented by four indices (*hkil*) and the zone axes of the patterns are represented by three indices [*uvw*].

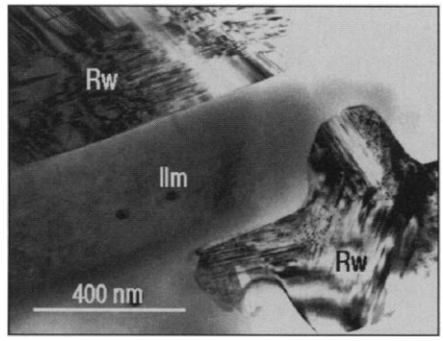

Fig. 5. Bright-field TEM image of intergrown $MgSiO_3$-ilmenite (Ilm) and ringwoodite (Rw). The mutual embayment of the $MgSiO_3$-ilmenite and the lower ringwoodite suggests simultaneous crystallization.

of melt veins in Acfer 040 probably began at a pressure and temperature in excess of 26 GPa and 2000°C. The presence of ilmenite demonstrates that shock-induced melt veins in chondrites continue to provide natural examples of important high-pressure minerals.

REFERENCES AND NOTES

1. E. A. Ringwood, *Composition and Petrology of the Earth's Mantle* (McGraw-Hill International Series in the Earth and Planetary Sciences, McGraw-Hill, New York, 1975), and references therein concerning synthesis of high-pressure minerals.
2. J. J. Gurney, *Diamonds in Kimberlites and Related Rocks*, vol. 2, *Geol. Soc. Am. Spec. Publ. 14, Proc. 4th Int. Kimberlite Conf.* (Blackwell, Oxford, 1989), p. 935.
3. R. A. Binns, R. J. Davis, S. J. B. Reed, *Nature* **221**, 943 (1969).
4. B. Mason, J. Nelen, J. S. White, *Science* **160**, 66 (1968).
5. J. V. Smith and B. Mason, *ibid.* **168**, 832 (1970).
6. A. Putnis and G. D. Price, *Nature* **280**, 217 (1979).
7. M. Chen and A. El Goresy, *Meteoritics* **29**, 456 (1994).
8. C. M. Lingemann and D. Stöffler, *ibid.* **29**, 491 (1994); *Lunar Planet. Sci.* **XXVI**, 851 (1995).
9. F. Langenhorst, P. Joreau, J.-C. Doukhan, *Geochim. Cosmochim. Acta* **59**, 1835 (1995).
10. M. Chen, T. G. Sharp, A. El Goresy, B. Wopenka, X. Xie, *Science* **271**, 1570 (1996).
11. C. M. Lingemann, F. Langenhorst, D. Stöffler, *Meteoritics* **30**, 537 (1995).
12. L.-G. Liu, *Geophys. Res. Lett.* **1**, 277 (1974).
13. N. Kawai, M. Tachimori, E. Ito, *Proc. Japan Acad.* **50**, 378 (1974).
14. L.-G. Liu, *Earth Planet. Sci. Lett.* **31**, 200 (1976).
15. M. Chen, T. G. Sharp, A. El Goresy, B. Wopenka, X. Xie, *Lunar Planet. Sci.* **XXVII**, 211 (1996); M. Chen, B. Wopenka, A. El Goresy, T. G. Sharp, *Meteoritics* **31**, A27 (1996).
16. T. G. Sharp, M. Chen, A. El Goresy, *Lunar Planet. Sci.* **XXVII**, 1175 (1996); *Meteoritics* **31**, A127 (1996).
17. A. Bischoff and T. Geiger, *Meteoritics* **30**, 113 (1995).
18. D. Stöffler, K. Keil, E. R. D. Scott, *Geochim. Cosmochim. Acta* **55**, 3845 (1991).
19. Polished thin sections of 20 μm thickness were used for optical, SEM, and microprobe investigations. Selected regions were then removed and prepared for TEM by ion-bombardment thinning. In order to minimize the damage to unstable compounds that can occur from heating and ion bombardment, the samples were prepared without the use of thermal adhesives, and ion milling was done using a liquid-nitrogen-cooled specimen holder. The low-temperature sample-preparation techniques were applied to samples studied in Bayreuth as well as selected samples studied previously in Münster. TEM was performed using Philips CM20 and CM20-FEG instruments operated at 200 kV, and both instruments were equipped with Noran Voyager analytical systems for energy-dispersive x-ray spectroscopy (EDS).
20. G. L. Nord Jr. and C. A. Lawson, *Am. Mineral.* **74**, 160 (1989).
21. P. E. Champness and G. W. Lorimer, *J. Mat. Sci.* **8**, 467 (1973); G. W. Lorimer and P. E. Champness, *Am. Mineral.* **58**, 243 (1973); G. L. Nord Jr., J. S. Huebner, M. Ross, *Lunar Planet. Sci.* **VIII**, 732 (1977); G. L. Nord Jr., *Phys. Chem. Miner.* **6**, 109 (1980).
22. S. Heinemann, T. G. Sharp, F. Seifert, D. C. Rubie, *Phys. Chem. Miner.* **24**, 206 (1997).
23. D. Hugh-Jones, T. Sharp, R. Angel, A. Woodland, *Eur. J. Mineral.* **8**, 1337 (1996); D. A. Hugh-Jones and R. J. Angel, *Am. Mineral.* **79**, 405 (1994); D. A. Hugh-Jones, A. B. Woodland, R. J. Angel, *ibid.* **79**, 1032 (1994).
24. T. Irifune, *Nature* **370**, 131 (1994).
25. Y. Wang, F. Guyot, R. Liebermann, *J. Geophys. Res.* **97**, 12327 (1992).
26. C. M. McCammon, D. C. Rubie, C. R. Ross II, F. Seifert, H. St. C. O'Neill, *Am. Mineral.* **77**, 894 (1992).
27. H. Mori, *J. Mineral. Soc. Japan* **23**, 171 (1994).
28. C. B. Agee, *Nature* **346**, 834 (1990); C. B. Agee, J. Li, M. C. Shannon, S. Ciercone, *J. Geophys. Res.* **100**, 17725 (1995).
29. T. Irifune, T. Koizumi, J.-I. Ando, *Phys. Earth Planet. Inter.* **96**, 147 (1996).
30. S. E. Kesson, J. D. FitzGerald, J. M. G. Shelley, *Nature* **372**, 767 (1994).
31. J. Zhang and C. Herzberg, *J. Geophys. Res.* **99**, 17729 (1994).
32. T. Gasparik, *ibid.* **97**, 15181 (1992).
33. M. J. Toplis, G. Libourel, M. R. Carrol, *Geochim. Cosmochim. Acta* **58**, 797 (1994).
34. M. Chen, B. Wopenka, A. El Goresy, T. G. Sharp, *Meteoritics* **29**, 98 (1996).
35. T. G. Sharp, M. Chen, A. El Goresy, *Lunar Planet. Sci.* **XXVIII**, 1283 (1997).

36. We thank two anonymous reviewers for helpful suggestions in the improvement of the manuscript. This work is part of a Ph.D. thesis (C.M.L.) at the Institut für Planetologie, Westfälische Wilhelms-Universität, Münster. It was partially supported by the Deutsche Forschungsgemeinschaft (DFG).

11 March 1997; accepted 19 June 1997

The Ionosphere of Europa from Galileo Radio Occultations

A. J. Kliore,* D. P. Hinson, F. M. Flasar, A. F. Nagy, T. E. Cravens

The Galileo spacecraft performed six radio occultation observations of Jupiter's Galilean satellite Europa during its tour of the jovian system. In five of the six instances, these occultations revealed the presence of a tenuous ionosphere on Europa, with an average maximum electron density of nearly 10^4 per cubic centimeter near the surface and a plasma scale height of about 240 ± 40 kilometers from the surface to 300 kilometers and of 440 ± 60 kilometers above 300 kilometers. Such an ionosphere could be produced by solar photoionization and jovian magnetospheric particle impact in an atmosphere having a surface density of about 10^8 electrons per cubic centimeter. If this atmosphere is composed primarily of O_2, then the principal ion is O_2^+ and the neutral atmosphere temperature implied by the 240-kilometer scale height is about 600 kelvin. If it is composed of H_2O, the principal ion is H_3O^+ and the neutral temperature is about 340 kelvin. In either case, these temperatures are much higher than those observed on Europa's surface, and an external heating source from the jovian magnetosphere is required.

The Galileo spacecraft is in orbit about Jupiter, studying Jupiter and the Galilean satellites (Io, Europa, Ganymede, and Callisto). Of these, only Io was known to have an atmosphere, which was observed by a radio occultation (*1*) of Pioneer 10 in 1973 (*2*). Observations and theoretical considerations suggest that Europa may have an atmosphere that originates from frozen surface water ice, most likely produced by particle impact (*3*, *4*). Therefore, any atmosphere must consist of some mixture of H_2O, H, H_2, OH, O_2, and O. Early Pioneer 10 observations suggested an atomic oxygen column density of around 1×10^{13} cm^{-2} (*5*), but these measurements may have been contaminated. Recent Hubble Space Telescope (HST) observations of the 1304–1356 Å lines of atomic oxygen were used to deduce an O_2 column density of about 1.5×10^{15} cm^{-2} (*6*). Recent Galileo measurements at Ganymede and Callisto indicated the presence of atomic hydrogen, with densities on the order of 1×10^4 cm^{-3} (*7*), which might suggest similar abundances at Europa.

A search for an atmosphere on Europa was carried out when Galileo was occulted by Europa three times: on 19 December 1996 (E4) and on 20 and 25 February 1997 (E6a and E6b). The parameters defining the properties of these occultations are given in Table 1. For a few minutes before and after the occultations, the S band (2.295 GHz, or about 13 cm wavelength) radio signal from Galileo traversed regions above Europa's surface in which one could observe the effects of refraction by an atmosphere, or more precisely, an ionosphere (a layer of ions and electrons produced in tenuous regions of the atmosphere by photoionization and magnetospheric particle impact), should one exist on Europa. Thus, the three occul-

A. J. Kliore, Jet Propulsion Laboratory, California Institute of Technology, Pasadena, CA 91109, USA.
D. P. Hinson, Center for Radar Astronomy, Stanford University, Stanford, CA 94305, USA.
F. M. Flasar, Laboratory for Extraterrestrial Physics, NASA/Goddard Space Flight Center, Greenbelt, MD 20771, USA.
A. F. Nagy, Space Physics Research Laboratory, University of Michigan, Ann Arbor, MI 48109, USA.
T. E. Cravens, Department of Physics and Astronomy, University of Kansas, Lawrence, KS 66045, USA.

*To whom correspondence should be addressed.